ADDITIVE MANUFACTURING OF BONE-INSPIRED STRUCTURAL-POWER COMPOSITES

J. Plocher, C. Lee, and A. Panesar*
Department of Aeronautics, Imperial College, London, United Kingdom
* Corresponding author (a.panesar@imperial.ac.uk)

Keywords: *Additive manufacturing; Multifunctional composite; Topology optimization; Medial axis transformation; Biomimicry*

ABSTRACT

Design for additive manufacturing today – benefitting from unprecedented geometrical freedom – is increasingly exploiting means of structural optimization, including topology optimization, latticing and by taking inspiration from nature. This paper constitutes a case study, highlighting the added value and potential of combining these structural design approaches in AM, particularly in terms of multifunctionality. A method to obtain bone-inspired structural-power composites, designed for fibre-reinforced additive manufacturing, with both high stiffness-to-weight ratio and ionic conductivity is presented. For this purpose, a sandwich structure with reinforced shell (compact bone) and lattice core (spongy bone) filled with ionic liquid (bone marrow) is proposed. A finite element analysis and calculations based on a resistance network model provided insight into the change and trade-off between mechanical and electrical performance with increasing shell thickness i.e. level of reinforcement. Investigations into fibre angle assignments following the central difference scheme and the medial axis transformation have shown comparable performance, providing ways of controlling and tailoring deposition paths to best meet requirements associated with the manufacturing with short and continuous fibre-reinforcements. The model with continuous fibre-reinforcement has shown great potential for improving the specific stiffness compared to the isotropic functional counterpart used as benchmark, while additionally providing the potential for energy storage, constituting a promising theoretical approach as to how AM can serve as means for lightweighting through functional integration. It was concluded, that in pursuit of improving the efficient material usage, tailored shell-infill designs should be considered in the future.

1 INTRODUCTION

Additive manufacturing (AM) today is enabling means of design and structural optimization which are infeasible for most other fabrication processes. Unique capabilities include the exact placement of material, facilitating the creation of intricate structures with cavities or undercuts as well as the opportunity to utilize mathematically-driven structural optimization methods like topology optimization (TO) or latticing. Multifunctionality represents a unique selling point for AM, exploiting the inherent design freedom and ultimately paving the way for more efficient structures. With approaches reaching from conductive inks [1–3] or the placement of electronics [4–7], to designs derived from multi-objective optimization [7,8], specifically capitalizing on mathematically-driven lightweighting strategies, research in this field is diverse. Besides, lattices are increasingly being used for light AM-parts, providing among high strength-to-weight ratios [9,10], energy- [11–15] and heat-dissipation [16–18]. Both TO and lattices lend themselves for tailoring the permeability [19–21], hence they can be considered promising from potential energy storage structures or structural power composites (SPCs) [22,23].

Design for AM (DfAM) i.e. considerations that ensure the manufacturability by employing either performance- or economically-driven constraints (e.g. consideration of infill patterns or support volume, respectively), are becoming increasingly important [24,25]. Digital AM and the process of transferring a geometry into an STL (stereolithography) file through slicing is representing a key aspect of this research. Today's slicing software commonly follow the shell-infill approach as a default setting,

meaning the imported structure is being printed using a set number of shell layers with a porous infill. An abundance of generic infill-patterns is at the engineer's disposal; however, none are actually tailored for the specific load profile of the part.

In light of structural optimization, deposition path planning is, therefore, representing an increasingly important aspect of DfAM for enhanced part performance. Particularly, FDM can use the process-induced anisotropy to their advantage if process and design are reconciled. In the quest for enhanced structural performance, multi-material printing, particularly fibre-reinforced AM (FRAM) with short (S-FRAM) and continuous (C-FRAM) fibres, are gaining interest [26–28]. An infill-pattern derived from the medial axis transformation has recently been identified as promising, as it allows gap-free manufacturing [29] and alignment with the principle load trajectories [30]. In combination with the above-mentioned design optimization approaches geared towards AM, there is scope for multifunctional lightweight parts in in which the system is an intrinsic part of the structure.

Biomimicry has become a trending topic in engineering over the last decade, providing a portfolio of light and robust architectures. The unique microstructures in natural composites, often characterized by strong and weak building blocks spanning over multiple length scales (hierarchical levels), offer great mechanical performance by combining commonly competing mechanical quantities such as stiffness and strength [31]. An increasing number of studies have employed AM to replicate bio-inspired structures [32], including e.g. bone [33–35].

This work investigates the specific stiffness and ionic conductivity of a bone-inspired SPC that is designed for a dual-nozzle printer setup capable FRAM (see Figure 1). A density-based topology optimisation was employed to obtain the geometrical layout (macrostructure) from which a sandwich structure with a fibre-reinforced shell and a lattice core is derived. Two methods for the assignment of fibre angles in the shell are investigated and compared. Assuming both a short and continuous fibre-reinforcement, a finite element analysis was conducted determining the stiffness-to-weight ratio with a change in shell thickness. The cavities within the isotropic lattice are defined as a reservoir for ionic liquid, providing energy storage capacity. A resistance network model was employed to calculate the ionic conductivity with increasing shell thickness. This case study showcases the potential of AM for multifunctionality, combining state-of-the-art lightweighting strategies and FRAM with a bio-inspired design approach.

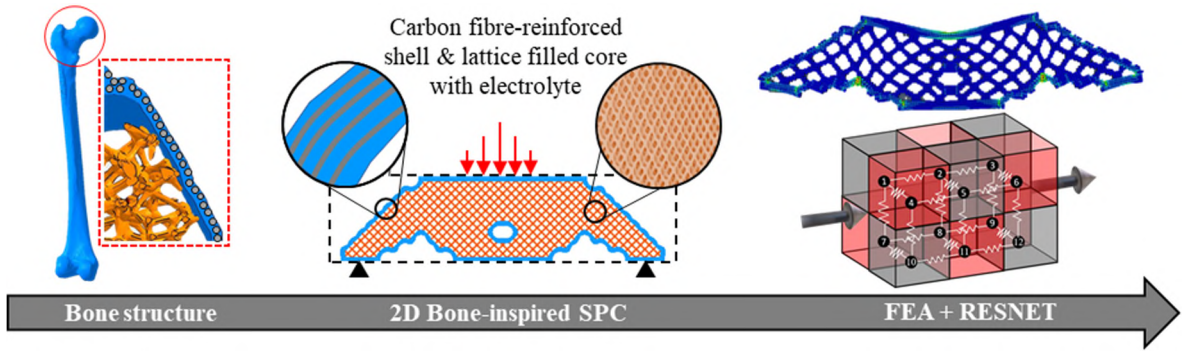

Figure 1: Bone-inspired design approach to lightweight SPCs for FRAM, followed by a performance evaluation through finite element analysis (FEA) and calculations based on a resistance network model (RESNET).

2 METHODOLOGY

Motivated by the reduction of weight through TO and functional integration, this work aims to develop a bone-inspired SPCs, replicating the following features as illustrated in Figure 2: 1) Dense cortical bone, accommodating the cylindrical osteons and predominantly providing strength and stiffness; 2) Spongy trabecular bone, taking on both metabolic functions and structural functions (energy absorption, buckling resistance, etc.); 3) Gelatinous bone marrow, producing red blood-cells, but contributing little structurally [36,37]. The analogous artificial bone structure is composed of the corresponding phases:

1) Short/Continuous fibre-reinforced shell; 2) Porous, isotropic lattice-microstructure; 3) Ionic liquid filling the void space in the cellular structure.

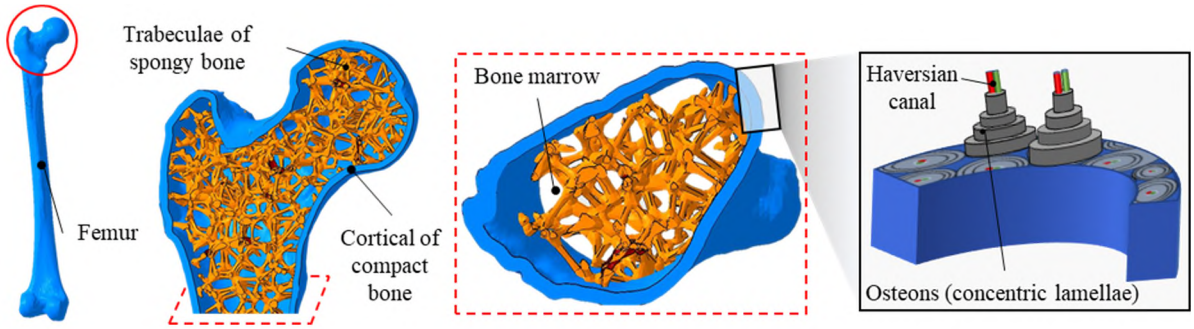

Figure 2: Schematic of the bone structure of a human femur, showcasing the essential components that are replicated for the SPC.

For this study, an extruded 2D problem was considered whereby the macrostructure is obtained using TO. A three-point bending scenario in line with ASTM D7264/D7264M-15 [38] with a symmetrically distributed load of 1N around the mid-plane and across five nodes was considered for a more realistic simulation of the experiment. A shell- and lattice domain was subsequently derived, and fibre angles were assigned using the central difference scheme (CDS) and medial axis transformation (MAT). As this design approach envisages to combine high specific stiffness with high electrical power, the part performance is finally assessed using a finite element analysis (FEA) and an analysis based on resistance network model (RESNET). The corresponding flowchart is illustrated in Figure 3. For manufacturing a dual-nozzle 3D-printer like the *MarkTwo* (*Markforged, Inc.*) [39], capable of printing polymer together with either S-FRAM or C-FRAM, was considered. A numerical analysis of the mechanical and electrochemical performance concludes this study.

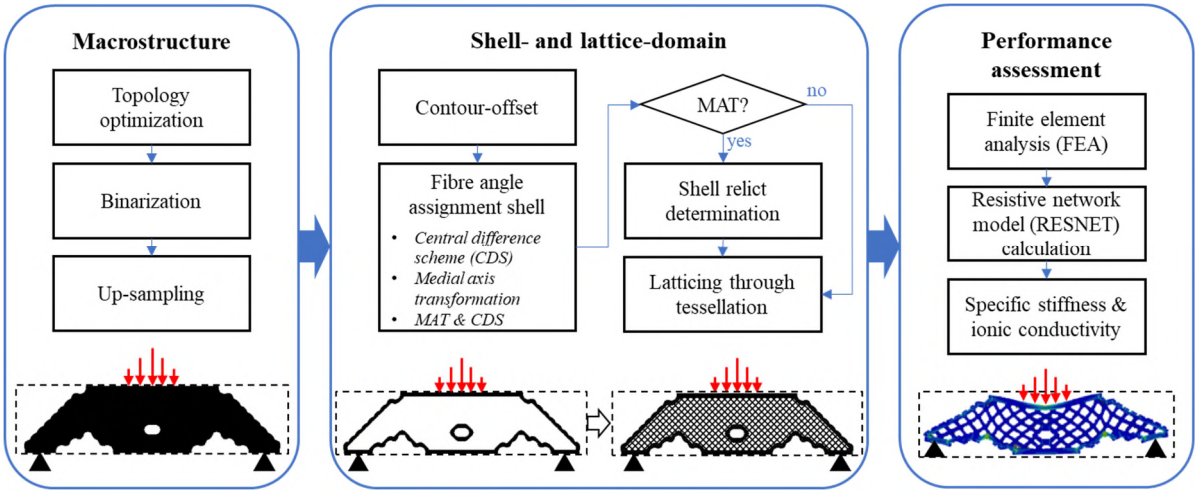

Figure 3: Flowchart showcasing the iterative process for the retrieval of the bone-inspired sandwich structure, designed for FRAM.

2.1 Macrostructure

A 2D macrostructure was obtained from the density-based TO method SIMP (Solid Isotropic Material with Penalization), which is centred on the power law approach and is aimed at minimizing compliance C (i.e. maximizing stiffness) for a given volume fraction $V(x)$. The objective function of this method is formulated as follows with the density x as a design variable

$$\min_x C(x) = U^T K U = \sum_{i=1}^{N} (x_i)^p u_i^T k_e u_i$$
$$subject\ to: \frac{V(x)}{V_0};\ \mathrm{KU} = \mathrm{F};\ 0 < x_{min} \leq x \leq 1; \qquad \text{Eq.1}$$

where U and K are the global displacement and stiffness matrices, which can be expressed as sum of the elemental pendants u_i and k_e. For this study, a penalization factor of $p = 3$ and volume fraction constraint of 70% was chosen. A true solid-void image from the greyscale SIMP-solution was subsequently obtained through a thresholding scheme that adjusts the density-limit at which an element is regarded as solid to best adhere to the initial volume fraction constraint. Finally, the resolution was increased from 40x10 to 400x100 elements to obtain more accurate FEA-results.

2.2 Shell structure

2.2.1 Contour-offset with fibre-angle assignment

Initially, the boundaries of the original topology were identified i.e. the outer perimeter and any holes that have formed within the structure. A shell structure was obtained through an erosion procedure (subtraction of the eroded structure from the original structure using a disk as morphological structuring element). A minimum shell thickness of three elements was chosen to obtain reliable results from the FEA. Subsequently, the shell thickness was iteratively increased by increments of one (contour-offset). This process was terminated before the approaching boundaries would overlap.
Similar to sandwich structures, the fibre placement in the outer shell is intended to improve the bending stiffness. Different material and fibre angle configurations i.e. deposition path strategies for a printer with a dual-nozzle setup are compared. This allows for combining unreinforced polymers with S-FRAM or C-FRAM in one part. Fibre angles for each element in the shell were assigned either according to CDS or MAT as shown in Figure 4.

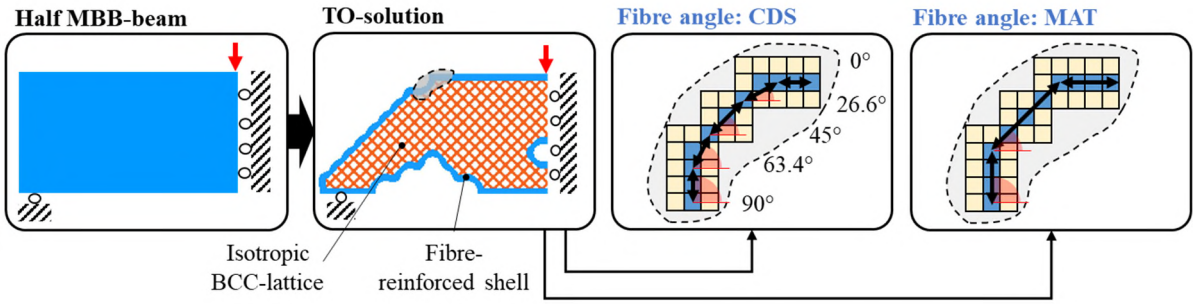

Figure 4: Topology optimized half MBB beam with bone-inspired architecture illustrating the fibre angle assignment according to the CDS and MAT method.

Central Difference Scheme (CDS): For this method each shell layer is examined separately. Individual shell elements are first identified, and angles are then assigned according to the position of the neighbouring elements in a 3x3 neighbourhood. This method lends itself for S-FRAM, as the fibre angle changes element-wise. Angles obtained with CDS can be calculated using:

$$\frac{\partial u}{\partial x}(\bar{x}) \cong \frac{u(\bar{x}+\Delta x) - u(\bar{x}-\Delta x)}{2\Delta x} \qquad \text{Eq.2}$$

Where Δx represents the fixed grid size which is dictated by the mesh. A quarter-model is shown in Figure 4, illustrating a set of possible angles that can be derived from the neighbouring elements in a 3x3x3 domain ($\tan^{-1}(0)$; $\tan^{-1}(0.5)$; $\tan^{-1}(1)$; $\tan^{-1}(2)$; $\tan^{-1}(\mathrm{Inf})$; etc.).

Medial Axis Transformation (MAT): This work employs a skeletonisation approach presented in [30], which centres on the thinning algorithm introduced in [7,40]. Information on nodes/branch-points, slopes or connectivity are derived from this process, allowing for a local fibre-angle assignment. As the medial axis is established iteratively starting from one node and progressing in the direction dictated by the topology, results can be ambiguous for symmetric topologies and were therefore mirrored in this study. Additionally, this process naturally results in spurs which were eliminated to obtain an unambiguous topology information. The medial axis was then further segmented using a minimum step size of five elements and a threshold angle of 20° degrees, introducing additional nodes and hence a more accurate representation of the local slopes. In contrast to CDS, the MAT approach considers all shell layers in the vicinity of each sub-link at once by dilating the medial axis (disk as morphological structuring element) up to the boundaries of the shell in pursuit of identifying the neighbouring elements of each sub-link and assigning the corresponding fibre angles corresponding to its slope. At the nodes, where it comes to an overlap of these domains, the mean fibre angle between the adjacent sub-links was assigned, providing a smooth angle transition. It is worth noting, that the MAT approach produces relicts in the "corners" of the shell (see Figure 4), which are not filled by the dilated skeleton (necessary to preserve equidistant deposition paths) and are therefore assigned isotropic properties. Similarly, due to the ambiguous nature of the medial axis in the voxel environment, the dilation process can result in excess elements i.e. elements that do not coincide with the original shell. These elements were removed to preserve the original shell domain. Moreover, due to the definition, that only more than 3 elements within one plane of a 3x3 square make up a node, loops can be created with no link and nodal information (e.g. internal hole in the structure under investigation in this work). In this case, the CDS method was automatically used instead.
This fibre angle assignment method lends itself better for C-FRAM, providing greater customizability in terms of the segmentation of the skeleton and hence the local fibre angle. Control over the sub-link lengths, enables a more continuous deposition path, facilitating the manufacturing with continuous fibres.

2.3 Core structure

The internal core domain was filled with a tessellated isotropic body-centred-cubic (BCC) lattice, using a standard Boolean operation (between original structure and the shell). The minimum strut thickness was set to three elements, ensuring a reasonable mesh size for the FEA. The volume fraction of the unit cell was set to 52%, meaning the tessellated lattice-core is going to result in volume fraction within the same range (deviations due to iterative change in shell thickness). It is of note, that for this work only x-shaped unit cells were employed (extruded 2D topology) to obtain FEA results, meaning an ionic fluid flow, as is the case in true 3D BCC-unit cells, was not considered.

2.4 Performance assessment

2.4.1 Finite element analysis (FEA) – Structural performance

FEA was conducted with Abaqus/CAE2018 [41], using reduced integration on an eight-node brick element. In line with the envisaged print materials nylon as well as short (SFR) and continuously (CFR) carbon fibre reinforced nylon was considered. The tensile moduli and densities used for the model were obtained from *Markforged Inc.* [42]. The Poisson's ratios were attained from *CES EduPack* software (Granta Design Ltd.) [43] and the shear moduli were derived thereof employing the known relationship $E = 2G(1+\nu)$. The values used are detailed in Note: *Values derived from ˣ Markforged Inc.[45]; ✡ CES EduPack [43]; * ratio E = 2G(1+ν).*. Void-regions have been assigned negligibly low properties to ensure minimal influence on the FEA result. It is of note, that the properties provided by *Markforged Inc.* deviate from e.g. [44] and are greatly dependent on the infill pattern.

*Note: Values derived from ˣ Markforged Inc.[45]; ✡ CES EduPack [43]; * ratio E = 2G(1+ν).*

Material parameters	Nylon	Short carbon fibre-reinforced nylon (SFR)	Continuously carbon fibre-reinforced nylon (CFR)	Void
E_1 [GPa]	0.94ˣ	1.4ˣ	60ˣ	0.1
E_2 [GPa]		0.94ˣ		
E_3 [GPa]				
ν_{12} [/]	0.34✡ (Pure PA6)	0.34✡ (PA6 with 30% PAN CF)		0.34
ν_{13} [/]		0.34✡ (Pure PA6)		
ν_{23} [/]				
G_{12} [GPa]	0.63*	0.52*	22.39*	0.03
G_{13} [GPa]		0.35*		
G_{23} [GPa]				
ρ [g/cm^3]	1.1	1.2	1.4	NA

Table 1: List of the print material properties used for the finite element model.

2.4.2 Resistance network model (RESNET) – Electrochemical performance

Filled with ionic liquid, the cavities in the lattice naturally provide energy storage capacity. This is proportional to the available volume, which is decreasing with the higher shell thickness. This study, however, is focusing on the ionic conductivity i.e. how the change in the topology of the internal domain influences the resistance. For this purpose, the RESNET model as presented by Rhazaoui et al. [46] is used, measuring the lowest resistance between two plate electrodes placed at the height of the two support points (see Figure 5a). The blue regions in Figure 5 represent either shell or void domains, which are assigned a resistance that is 10^3 times higher than that of the electrolyte. The internal lattice structure is homogenized (yellow domain), meaning the effective conductivity is determined from the relative density. Based upon Kirchhoff's laws, the RESNET model centres on determining the resistance R between adjacent elements (i^{th} and j^{th} element) that are arranged in series. The resistances between the shared faces are hereby differentiated into inter-elemental or between element and electrode:

$$R_{ij} = \alpha_i R_i + \alpha_j R_j, \qquad \alpha = \begin{cases} 1/2 & for\ internal\ elements \\ 1 & for\ boundary\ elements\ (electrode) \end{cases} \qquad \text{Eq.3}$$

The global ionic conductivity is subsequently calculated as the sum of the inverse resistances. Figure 5b illustrates the corresponding RESNET model composed of two different materials where the arrows indicate the direction of the current. As an uninterrupted current flow is only possible for a true 3D lattice, this study assumes that the lattice domain is empty, providing solely a prove of concept and not the actual conductivity values.

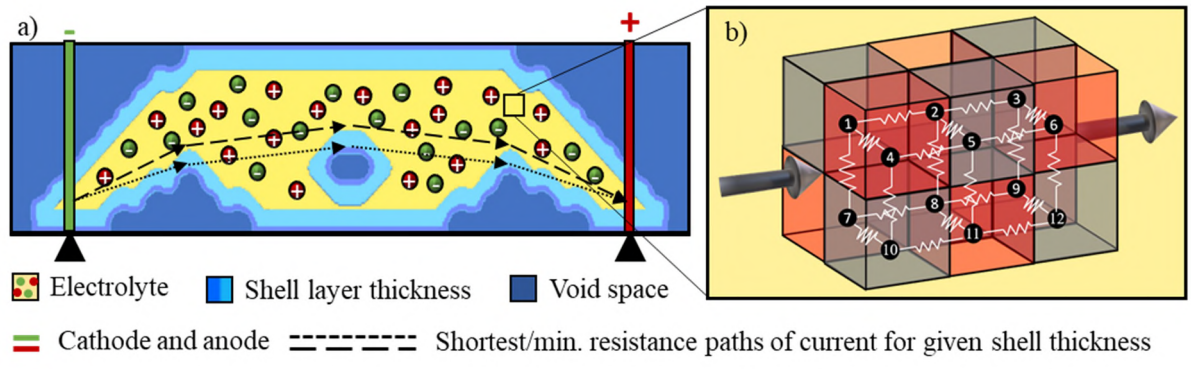

Figure 5: a) Shell structure illustrating extreme values for shell thickness, electrolyte domain and electrode placement. b) Resistance network model as proposed in [46].

3 RESULTS AND DISCUSSION

Figure 6 illustrates the change in the mechanical and normalized electrical performance with increasing shell thickness, as obtained from the FEA and the RESNET model, respectively. The former is presented as specific stiffness, calculated from the sum of the strain energies divided by the weight of the composite (dependent on composite configuration and does not account for the weight of the electrolyte). On the contrary, the ionic conductivity was normalized based on maximum electrical performance i.e. when the shell thickness is the lowest. It is of note that the medial axis information could only be obtained for the outer perimeter, the fibre angles in the internal shell were all assigned using CDS. For reference, the specific stiffness of the baseline functional structure (BFS) with entirely isotropic properties was included (see Figure 6).

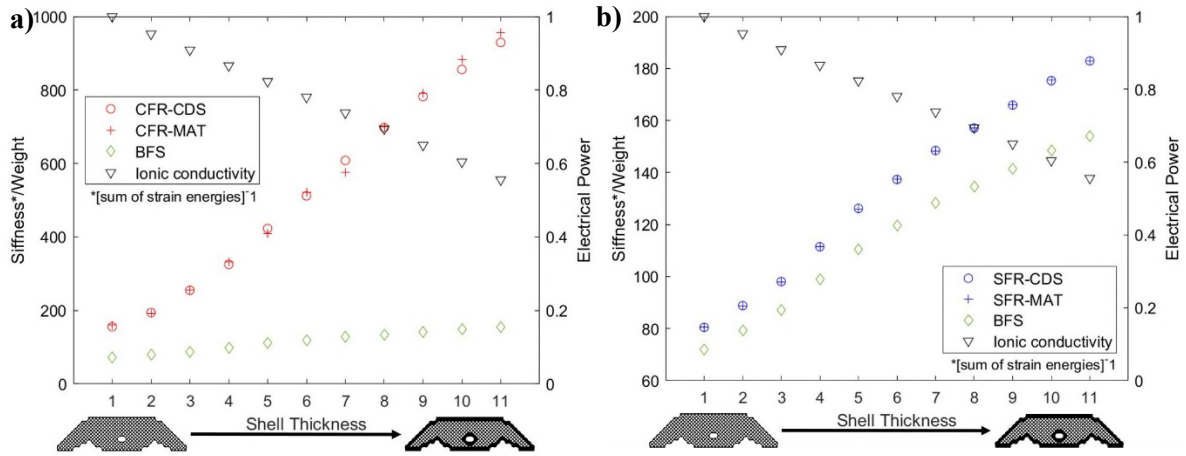

Figure 6: Change of the stiffness-to-weight ratio and electrical power of the bone-inspired SPCs with a change in shell thickness for a) continuously and b) short fibre-reinforced materials (SFR and CFR) and fibres assigned with either CDS or MAT.

A sixfold greater increase in specific stiffness (i.e. curve of specific stiffness) with shell thickness/reinforcement content was determined for the continuously fibre-reinforced composite, compared to the short-fibre counterpart. It is worth noting, however, that the specific modulus of the continuous fibre-reinforced material is 37 times higher (see Table 1) than that of the short fibre. A reason why this is not reflected in the difference between the specific stiffness values could be e.g. the use of in-plane properties for a loading case which is bending-dominated, or the calculation of stiffness based on strain energy. Figure 6 illustrates that maximum ratio of the specific stiffness between BFS:CFR and BFS:SFR is 1:6.2 and 1:1.2, respectively. The corresponding ratios between the material properties of pure polymer to continuous and short fibre-reinforced polymers (see Table 1) are 1:50.2 and 1:1.4, respectively. This leads to conclude, that the location of the reinforced material within the shell is not stiffness-optimal for this scenario and should be reconsidered. It would, therefore, be of interest to develop slicing algorithms that employ e.g. tailored lattices or introduce additional load-bearing internal shells to improves the specific stiffness. While lattices are used here to provide permeability with some load-bearing capabilities, a conventional shell-infill configuration may not be ideal for SPCs. However, despite the reduction of specific stiffness that requires attention in the design process, it is worth noting, that an improved buckling load [47] or greater robustness [48,49] are also associated with porous infills, potentially presenting an acceptable trade-off.

Overall, good agreement between the mechanical performance of the composites designed using CDS or MAT were found – only minor deviations were noticed for the use of continuous fibres. The segmentation of the medial axis is most likely the cause for that, as fibres are not strictly following the slope of the axis, like in CDS (see **Error! Reference source not found.**). In the latter fibre angles are assigned rigorously along the boundary contours whereas the segmentation in the MAT approach

assigns large domains the same angle, therefore, approximating the actual curvatures in the medial axis. The results are therefore greatly dependent on the segmentation parameters i.e. the step size and the threshold angle. As this approach is geared towards C-FRAM, a recursive segmentation would potentially improve the balance between precise geometrical reproduction, while preserving fabrication constraints, calling for minimal incidences of fibre angle changes per deposited fibre length (fewer undulations), potentially providing a more efficient force transfer. The MAT approach might in turn be beneficial for the manufacturability and favourable for large shell thicknesses compared to CDS. It is of note, that this aspect of DfAM is crucial for the final performance, which is why this study can only draw conclusions on the theoretical impact of fibre-reinforcement in the shell structure on the specific stiffness.

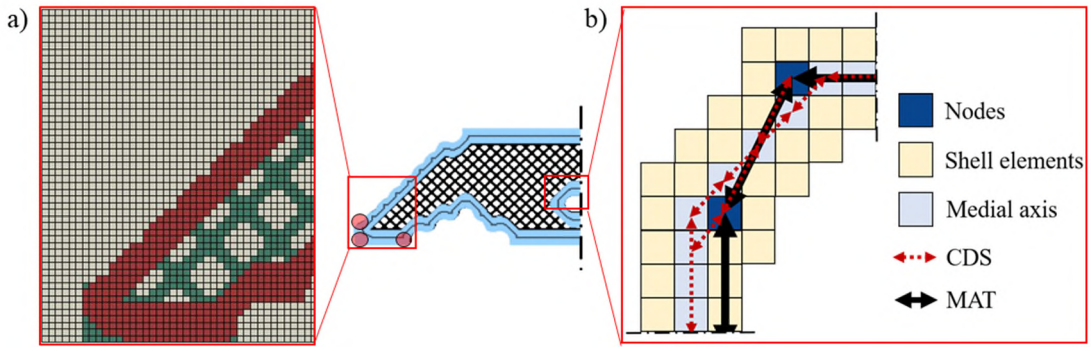

Figure 7: MAT-based fibre angle assignment causing a) shell relicts and b) a course approximation of the curvatures compared to CDS.

Error! Reference source not found. represents the decline in the specific stiffness with respect to fibre content (share of fibre-reinforced material from the total area, as defined by the original solid isotropic topology). The trend shows, that the weight increase predominates the stiffness gains. Even though the percentage gain is fairly constant for each iteration (about 3% increase with each additional shell layer), the specific stiffness drops more drastically for the first three iterations and then transitions into a much flatter slope. Constituting a bending-dominated test scenario, a fibre-reinforced shell is beneficial (high initial specific stiffness). However, despite the increases in the area moment of inertia with higher shell thickness, the stiffness gains cannot outweigh the weight-penalty through the added material, resulting in structures with increasingly lower specific stiffness. It is nevertheless noteworthy, that the reinforced structures are always outperforming the unreinforced BFS. Conclusively, our findings suggest that the contour offset method alone is not sufficient to provide high specific stiffness. This provides an incentive for research into tailored infills/lattices or the incorporation of anisotropic considerations into TO in the future.

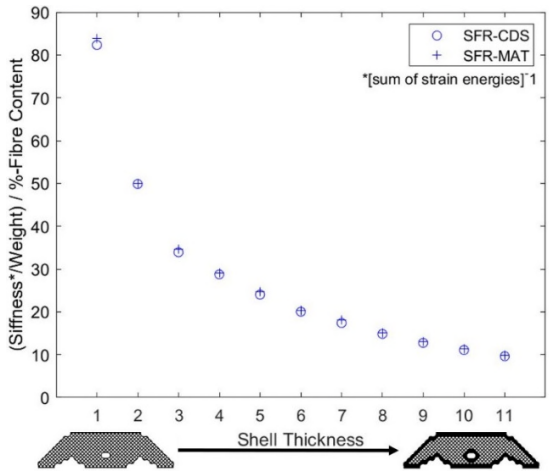

Figure 8: a) Change in specific stiffness of the shell-structure with increasing shell thickness for CDS and MAT in conjunction with SFR material.

Besides the decrease in the electrical capacity with increased shell thickness (not captured in Figure 6), a decline in ionic conductivity was observed, as the distance of the shortest path between the two electrodes increases, resulting in a higher resistance (see Figure 5). At the maximum shell thickness, only about 50% of the original conductivity value is achievable. A somewhat linear trend for the ionic conductivity was observed for this particular structure (see Figure 6). It is of note, in general, the change of conductivity is greatly dependent on the change in internal topology and must therefore not necessarily be linear. The same is true for the mechanical performance, as the geometrical layout is confined, the amount of additional fibre-reinforced material in each iteration is converging to zero with the proposed contour-offset approach. It can, therefore, be regarded as a typical multi-objective optimization problem, for which a sweet-spot can be determined based on specific trade-off requirements prescribed for the design.
It was shown, that this bone-inspired sandwich structure with fibre-reinforced shell and lattice core can help realize mass and volume savings to increase the specific stiffness in comparison to a purely isotropic counterpart while additionally providing scope for multifunctionality.

4 CONCLUDING REMARKS

This case study has demonstrated a method to obtain lightweight bone-inspired SPCs designed for AM, exploiting the design freedom AM has on offer and elucidating the promising potential for multifunctional designs. The methodology presented is not only composed of two state-of-the-art lightweighting strategies, namely latticing and density-based TO but also combines it with tailored fibre angle assignment strategies for FRAM with short and continuous fibres. With the premise to surpass the specific stiffness of a truly solid structure while adding functionality (ionic conductivity i.e. energy storage capability), a sandwich structure design with a continuously fibre reinforced shell has proven to be effective. On the contrary, the properties of the short fibres were found to provide only an insignifcant structural advantage over a purely isotropic functional structure and is therefore not able to compensate for the inherently low specific stiffness of lattices. With the central difference scheme (CDS) and the medial axis transformation (MAT), this study compared two fibre angle assignment schemes that provide customizability for the individual manufacturing constraints associated with short and continuous fibres. A resistance network model used to determine the change in electrical performance for increasing shell thickness, completed the insight into this classical trade-off study, assessing the multifunctional performance.
With the increased utility and development in electrical and unmanned aerial vehicles, for which weight and energy consumption are mutually dependent, these multifunctional SPCs inspired by nature could find great application in e.g. the external skin, providing robustness, stiffness, weight reduction and energy storage capabilities. These preliminary results suggest that AM lends itself greatly for these complex structures in which the system is an intrinsic part of the structure.
Current limitations, like an experimental verification (including tool path generation) or the design of a true 3D topology shall be the subject of future work. Extending this method for more advanced three-nozzle 3D-printers would be of interest, allowing greater customizability. In this context, the authors believe that an interesting extension to this work would be the investigation into tailored fibre-reinforced infill patterns (e.g. fibre-reinforced lattice cores) and the effect of different unit cells on the overall performance and conductivity of SPCs.

5 REFERENCES

[1] K. Chizari, M. Arjmand, Z. Liu, U. Sundararaj, D. Therriault, Three-dimensional printing of highly conductive polymer nanocomposites for EMI shielding applications, Mater. Today Commun. 11 (2017) 112–118. doi:10.1016/j.mtcomm.2017.02.006.

[2] Y. Lu, M. Vatani, J.W. Choi, Direct-write/cure conductive polymer nanocomposites for 3D

structural electronics, J. Mech. Sci. Technol. 27 (2013) 2929–2934. doi:10.1007/s12206-013-0805-4.

[3] J.J. Adams, E.B. Duoss, T.F. Malkowski, M.J. Motala, B.Y. Ahn, R.G. Nuzzo, J.T. Bernhard, J.A. Lewis, Conformal printing of electrically small antennas on three-dimensional surfaces, Adv. Mater. 23 (2011) 1335–1340. doi:10.1002/adma.201003734.

[4] C. Shemelya, F. Cedillos, E. Aguilera, D. Espalin, D. Muse, R. Wicker, E. Macdonald, Encapsulated copper wire and copper mesh capacitive sensing for 3-D printing applications, IEEE Sens. J. 15 (2015) 1280–1286. doi:10.1109/JSEN.2014.2356973.

[5] E. MacDonald, R. Wicker, Multiprocess 3D printing for increasing component functionality, Sci. Rev. 353 (2016). doi:10.1126/science.aaf2093.

[6] E. MacDonald, R. Salas, D. Espalin, M. Perez, E. Aguilera, D. Muse, R.B. Wicker, 3D printing for the rapid prototyping of structural electronics, IEEE Access. 2 (2014) 234–242. doi:10.1109/ACCESS.2014.2311810.

[7] A. Panesar, D. Brackett, I. Ashcroft, R. Wildman, R. Hague, Design framework for multifunctional additive manufacturing: placement and routing of three-dimensional printed circuit volumes, J. Mech. Des. – An Addit. Manuf. Spec. Issue. 137 (11) (2015) 111414/1-111414/10. doi:10.1115/1.4030996.

[8] B.S. Lazarov, O. Sigmund, K.E. Meyer, J. Alexandersen, Experimental validation of additively manufactured optimized shapes for passive cooling, Appl. Energy. 226 (2018) 330–339. doi:10.1016/j.apenergy.2018.05.106.

[9] X. Wendy Gu, J.R. Greer, Ultra-strong architected Cu meso-lattices, Extrem. Mech. Lett. 2 (2015) 7–14. doi:10.1016/j.eml.2015.01.006.

[10] M.C. Messner, Optimal lattice-structured materials, J. Mech. Phys. Solids. 96 (2016) 162–183. doi:10.1016/j.jmps.2016.07.010.

[11] T. Tancogne-Dejean, A.B. Spierings, D. Mohr, Additively-manufactured metallic micro-lattice materials for high specific energy absorption under static and dynamic loading, Acta Mater. 116 (2016) 14–28. doi:10.1016/j.actamat.2016.05.054.

[12] M. Vesenjak, L. Krstulović-Opara, Z. Ren, Ž. Domazet, Cell shape effect evaluation of polyamide cellular structures, Polym. Test. 29 (2010) 991–994. doi:10.1016/j.polymertesting.2010.09.001.

[13] C. Bonatti, D. Mohr, Large deformation response of additively-manufactured FCC metamaterials: From octet truss lattices towards continuous shell mesostructures, Int. J. Plast. 92 (2017) 122–147. doi:10.1016/j.ijplas.2017.02.003.

[14] P. Qiao, M. Yang, F. Bobaru, Impact Mechanics and High-Energy Absorbing Materials: Review, J. Aerosp. Eng. 21 (2008) 235–248. doi:10.1061/(ASCE)0893-1321(2008)21.

[15] M.R. O'Masta, L. Dong, L. St-Pierre, H.N.G. Wadley, V.S. Deshpande, The fracture toughness of octet-truss lattices, J. Mech. Phys. Solids. 98 (2017) 271–289. doi:10.1016/j.jmps.2016.09.009.

[16] A.O. Aremu, J. Brennan-Craddock, A. Panesar, I.A. Ashcroft, R.J.M. Hague, R.D. Wildman, C. Tuck, A voxel-based method of constructing and skinning conformal and functionally graded lattice structures suitable for additive manufacturing, Addit. Manuf. 13 (2017) 1–13. doi:http://doi.org/10.1016/j.addma.2016.10.006.

[17] E. Handler, A. Sterling, J. Pegues, H. Ozdes, M. Masoomi, Design and Process Considerations for Effective Additive Maufacturing of Heat Exchangers, in: Proc. 28th Annu. Int. Free. Fabr. Symp., Austin (Texas), 2017: pp. 2632–2640.

[18] L. Cheng, J. Liu, X. Liang, A.C. To, Coupling lattice structure topology optimization with

design-dependent feature evolution for additive manufactured heat conduction design, Comput. Methods Appl. Mech. Eng. 332 (2018) 408–439. doi:10.1016/j.cma.2017.12.024.

[19] M. Osanov, J.K. Guest, Topology Optimization for Architected Materials Design, Annu. Rev. Mater. Res. 46 (2016) 211–233. doi:10.1146/annurev-matsci-070115-031826.

[20] J. Guest, J. Prevost, Optimizing multifunctional materials: Design of microstructures for maximized stiffness and fluid permeability, Int. J. Solids Struct. 43 (2006) 7028–7047. doi:10.1016/j.ijsolstr.2006.03.001.

[21] J.K. Guest, J.H. Prévost, Design of maximum permeability material structures, Comput. Methods Appl. Mech. Eng. 196 (2007) 1006–1017. doi:10.1016/j.cma.2006.08.006.

[22] L.E. Asp, E.S. Greenhalgh, Structural power composites, Compos. Sci. Technol. 101 (2014) 41–61. doi:10.1016/j.compscitech.2014.06.020.

[23] C. Lee, E.S. Greenhalgh, M.S.P. Shaffer, A. Panesar, Design and characterisation of optimised microstructures for multifunctional structural, Prep. Submiss. to Adv. Funct. Mater. (2019).

[24] M. Kumke, H. Watschke, T. Vietor, A new methodological framework for design for additive manufacturing, Virtual Phys. Prototyp. 11 (2016) 3–19. doi:10.1080/17452759.2016.1139377.

[25] Y. Tang, Y.F. Zhao, A survey of the design methods for additive manufacturing to improve functional performance, Rapid Prototyp. J. 22 (2016) 569–590. doi:10.1108/RPJ-01-2015-0011.

[26] L.G. Blok, M.L. Longana, H. Yu, B.K.S. Woods, An investigation into 3D printing of fibre reinforced thermoplastic composites, Addit. Manuf. 22 (2018) 176–186. doi:10.1016/j.addma.2018.04.039.

[27] X. Wang, M. Jiang, Z. Zhou, J. Gou, D. Hui, 3D printing of polymer matrix composites: A review and prospective, Compos. Part B Eng. 110 (2017) 442–458. doi:10.1016/j.compositesb.2016.11.034.

[28] Z. Quan, A. Wu, M. Keefe, X. Qin, J. Yu, J. Suhr, J.H. Byun, B.S. Kim, T.W. Chou, Additive manufacturing of multi-directional preforms for composites: Opportunities and challenges, Mater. Today. 18 (2015) 503–512. doi:10.1016/j.mattod.2015.05.001.

[29] D. Ding, Z. Pan, D. Cuiuri, H. Li, N. Larkin, Adaptive path planning for wire-feed additive manufacturing using medial axis transformation, J. Clean. Prod. 133 (2016) 942–952. doi:10.1016/j.jclepro.2016.06.036.

[30] J. Plocher, A. Panesar, Next-Generation Fibre-Reinforced Lightweight Structures for Additive Manufacturing, in: 29th Annu. Int. Solid Free. Fabr. Symp., Austin, Texas, USA, 2018: pp. 664–684.

[31] A.R. Studart, Towards high-performance bioinspired composites, Adv. Mater. 24 (2012) 5024–5044. doi:10.1002/adma.201201471.

[32] A.R. Studart, Additive manufacturing of biologically-inspired materials, Chem. Soc. Rev. 45 (2016) 359–376. doi:10.1039/C5CS00836K.

[33] B.G. Compton, J.A. Lewis, 3D-printing of lightweight cellular composites, Adv. Mater. 26 (2014) 5930–5935. doi:10.1002/adma.201401804.

[34] J.J. Martin, B.E. Fiore, R.M. Erb, Designing bioinspired composite reinforcement architectures via 3D magnetic printing, Nat. Commun. 6 (2015) 1–7. doi:10.1038/ncomms9641.

[35] Q. Fu, E. Saiz, A.P. Tomsia, Bioinspired strong and highly porous glass scaffolds, Adv. Funct. Mater. 21 (2011) 1058–1063. doi:10.1002/adfm.201002030.

[36] J. Currey, Bones : Structure and mechanics, 2nd ed., Princeton, NJ : Princeton University Press, Oxfordshire, 2006.

[37] V.J. Vigorita, B. Ghelman, D. Mintz, Orthopaedic Pathology, 2nd ed., Lippincott Williams &

Wilkins, Philadelphia, 2008.

[38] ASTM, Standard Test Method for Flexural Properties of Polymer Matrix Composite Materials 1, Annu. B. ASTM Stand. (2010) 1–11. doi:10.1520/D7264.

[39] The Mark Two, Markforged, Inc. (2018). https://markforged.com/mark-two/ (accessed July 9, 2018).

[40] M. Kerschnitzki, P. Kollmannsberger, M. Burghammer, G.N. Duda, R. Weinkamer, W. Wagermaier, P. Fratzl, Architecture of the osteocyte network correlates with bone material quality, J. Bone Miner. Res. 28 (2013) 1837–1845. doi:10.1002/jbmr.1927.

[41] Dassault Systèmes. Abaqus CAE.(Version 2018) [Software] Dassault Systèmes, (2018). https://www.3ds.com/products-services/simulia/products/abaqus/abaquscae/ (accessed July 2, 2018).

[42] Material Datasheet - Composites, Markforged, Inc. (2019). http://static.markforged.com/downloads/composites-data-sheet.pdf (accessed May 4, 2019).

[43] "CES EduPack software, Granta Design Limited, Cambridge, UK, 2018 (www.grantadesign.com).," (2018).

[44] A.N. Dickson, J.N. Barry, K.A. McDonnell, D.P. Dowling, Fabrication of continuous carbon, glass and Kevlar fibre reinforced polymer composites using additive manufacturing, Addit. Manuf. 16 (2017) 146–152. doi:10.1016/j.addma.2017.06.004.

[45] Markforged Material Datasheet - Composites, Markforged, Inc. (2018). https://static.markforged.com/markforged_composites_datasheet.pdf (accessed May 14, 2019).

[46] K. Rhazaoui, Q. Cai, C.S. Adjiman, N.P. Brandon, Towards the 3D modeling of the effective conductivity of solid oxide fuel cell electrodes: I. Model development, Chem. Eng. Sci. 116 (2014) 781–792. doi:10.1016/j.ces.2014.05.045.

[47] A. Clausen, N. Aage, O. Sigmund, Exploiting Additive Manufacturing Infill in Topology Optimization for Improved Buckling Load, Engineering. 2 (2016) 250–257. doi:10.1016/J.ENG.2016.02.006.

[48] A. Panesar, M. Abdi, D. Hickman, I. Ashcroft, Strategies for functionally graded lattice structures derived using topology optimisation for Additive Manufacturing, Addit. Manuf. 19 (2018) 81–94. https://doi.org/10.1016/j.addma.2017.11.008.

[49] J. Wu, N. Aage, O. Sigmund, Infill Optimization for Additive Manufacturing – Approaching Bone-like Porous Structures, IEEE Trans. Vis. Comput. Graph. PP. 24 (2017) 1127–1140. doi:10.1109/TVCG.2017.2655523.